

## Article

# Thermal Effects of Electromagnetic Energy on Skin in Contact with Metal: A Numerical Analysis

Teerapot Wessapan <sup>1</sup>, Phadungsak Rattanadecho <sup>2</sup>, Nisakorn Somsuk <sup>3,\*</sup>, Manop Yamfang <sup>1</sup>, Manaporn Guptasa <sup>1</sup> and Prempreeya Montienthong <sup>4</sup>

- <sup>1</sup> Department of Mechanical Engineering, Faculty of Engineering, Rajamangala University of Technology Thanyaburi, Pathum Thani 12110, Thailand; teerapot\_w@rmutt.ac.th (T.W.); manop\_y@rmutt.ac.th (M.Y.); manaporn\_g@rmutt.ac.th (M.G.)
- <sup>2</sup> Center of Excellence in Electromagnetic Energy Utilization in Engineering (CEEE), Department of Mechanical Engineering, Faculty of Engineering, Thammasat University (Rangsit Campus), Pathum Thani 12120, Thailand; ratphadu@enr.tu.ac.th
- <sup>3</sup> Department of Industrial Engineering, Faculty of Engineering, Rajamangala University of Technology Thanyaburi, Pathum Thani 12110, Thailand
- <sup>4</sup> Department of Sustainable Development Technology, Faculty of Science and Technology, Thammasat University (Rangsit Campus), Pathum Thani 12120, Thailand; prempree@tu.ac.th
- \* Correspondence: nisakorn\_so@rmutt.ac.th

**Abstract:** It has been well recognized that interactions between electromagnetic fields and metals are very strong. The consequence of human tissue in contact with metal, when subjected to an alternating electromagnetic field, is an increase in tissue temperature, which results from metals absorbing the energy obtained through induction. However, the electromagnetic induction characteristics and tissue energy absorbed caused by various electromagnetic field exposure conditions have not been well understood. A computational model was developed and employed in this study to assess the temporal and spatial temperature increases in skin due to contact with a highly conductive metallic plate while subjected to a high-intensity electromagnetic field. The effects of plate material, plate thickness, coil distance, and exposure time on temperature increase in the skin were computationally investigated. The electromagnetic and temperature distributions in skin layers during exposure to electromagnetic fields were achieved using models of electromagnetic wave propagation and an unsteady bioheat transfer. The modeling approach used indicates that the plate thickness, plate material, coil distance, and exposure time have a significant impact on the temperature change in the skin. The most important parameter was found to be the metal type. Iron has the greatest effect on skin temperature increase when subjected to external electromagnetic induction. These results allow the researchers to estimate more precisely the exposure limits for induction coils.

**Keywords:** electromagnetic field; induction; skin tissue; bioheat transfer; wearable device



**Citation:** Wessapan, T.; Rattanadecho, P.; Somsuk, N.; Yamfang, M.; Guptasa, M.; Montienthong, P. Thermal Effects of Electromagnetic Energy on Skin in Contact with Metal: A Numerical Analysis. *Energies* **2023**, *16*, 5925. <https://doi.org/10.3390/en16165925>

Academic Editors: Hideaki Ohgaki and Boonyang Plangklang

Received: 25 June 2023

Revised: 31 July 2023

Accepted: 8 August 2023

Published: 10 August 2023



**Copyright:** © 2023 by the authors. Licensee MDPI, Basel, Switzerland. This article is an open access article distributed under the terms and conditions of the Creative Commons Attribution (CC BY) license (<https://creativecommons.org/licenses/by/4.0/>).

## 1. Introduction

Electromagnetic induction heating is a complex phenomenon in which electrically conductive material is placed nearby an alternating magnetic field source and heated by hysteresis (only magnetic materials) and/or induced electrical current (all conductive materials). An alternating current (AC) is fed via an electrical winding (coil/inductor) to produce the alternating magnetic field. One widespread misconception is that electromagnetic induction heating can only be used to heat magnetic components. However, induction heating can be used to heat any electrically conducting substance. Moreover, induction heating occurs without any physical contact between the material and the induction coil. The induction cooker is one example of an invention that makes use of induction heating. The coil is located at the base of the cooker, and its electromagnetic fields interact with the metal container. Because only high-conductivity materials can really be heated in this way,

the container warms up, whereas the hand on the cooktop remains comfortable. However, if wearing a wearable gadget or implanting highly conductive materials, the user may encounter undesired thermal consequences.

Wearable electronics and accessories, such as smart watches, bracelets, and earrings, are commonly utilized daily. These devices are made of highly conductive metal material, which generates an induced current when exposed to a strong electromagnetic field, producing induction heating, and potentially harming exposed areas such as the skin (Figure 1). As the popularity of wireless wearable and implantable devices grows, so does the requirement to address their safety [1]. Wearable gadgets containing metal may pose a danger of thermal harm from the electromagnetic induction effect, mostly owing to direct physical contact with human skin [2].

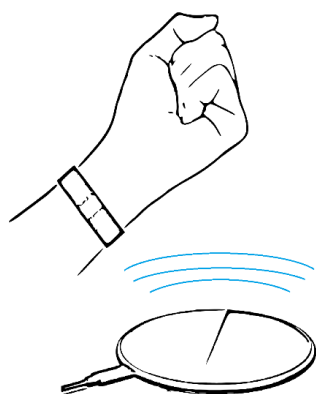


**Figure 1.** Wearable electronics and accessories made of highly conductive materials exposed to a strong electromagnetic field, resulting in induction heating.

In the past, comprehensive approaches for investigating heat-related skin injuries have been investigated. The researchers reported that the severity of the burns evaluated was impacted by both the temperature and the duration of exposure time. According to Johnson et al. [3], and the International Electrotechnical Commission (IEC) [4], the threshold temperature for producing skin damage is 43 °C. Some investigation has been conducted to attribute skin burn problems [5]. During simulated fires, the estimates of skin temperature distribution and heat flow were examined [6]. Heat stress and skin burns in firefighters' exposure to low-level thermal radiation were examined by Yang et al. [7]. Abraham et al. [8] provided a numerical method for estimating the depth of burns induced by high-temperature water exposure on human skin. According to the model, the burn extent appeared to spread into the epidermal and dermal layers at higher temperatures and longer exposure durations. Log [9] studied the temperature buildup and skin burning damages generated by simulated flare thermal exposures to exposed skin. Greater flare rates, corresponding to maximal flare heat transmission to the skin, were found to result in higher basal layer temperatures. Researchers have previously investigated skin injuries caused by contact with hot metal items [10–12]. Subramanian and Chato [10] developed thermal safety criteria for a general situation corresponding to skin interaction with a heated plate. Ng et al. [11] modeled the distribution of skin temperature during an interface with a heated object. Abraham et al. [12] investigated temperature distribution in skin because of heat exchange with a heated metallic medium.

Concerns have also been expressed that metal objects and devices in the vicinity of electromagnetic radiation might alter the absorption of electromagnetic energy and lead to temperature increases in the human body. Virtanen et al. [13,14] studied the influence of implant size, position, and orientation on the energy absorbed in tissues. They observed that implants inserted deeper into the body absorb much more than implants inserted close to the surface of the skin. Whittow et al. [15–18] conducted considerable research on the effects of metals on human tissue, primarily jewelry and spectacles. They observed that depending on the shape of the glasses and the operation frequency, wearing spectacles

can alter or boost the specific absorption rate in the eyes. Our previous works have also looked at the distribution of electric field, specific absorption rate (SAR), and heat transfer in different parts of the human body, such as the torso [19,20], head [21,22], eye [23,24], and so on [25–27], caused by encountering near- and far-field radiative elements. It has been revealed that the form of the radiating source, as well as its distance from the tissue, have an important influence on the absorption of electromagnetic radiation. Our previous work [22] discovered that the metal items near the head during electromagnetic field exposure change energy absorption and raise tissue temperature. Mathematical bioheat transfer modeling [28] has become essential in studying temperature in the human body. It finds application in various fields, including microwave liver ablation (MWA) [29] and simulating controlled drug delivery with thermo-sensitive liposomes [30]. Additionally, coupled models for tissue heterogeneity enhance pain relief techniques such as radiofrequency therapies [31]. Accurate heat transfer prediction through bioheat modeling advances medical techniques and mitigates unwanted thermal effects from different sources. However, research on the temperature of tissues in contact with metal objects during exposure to high-intensity electromagnetic fields is still sparse.

The contribution of different metals in contact with skin exposure to electromagnetic fields is essential for an adequate assessment of the temperature rise in tissue in association with metal induced by electromagnetic field exposures. The thermal response of skin in contact with a metal plate to electromagnetic energy was computed in this work. Based on the work of Ng et al. [11], a human skin model was built to determine the temperature increase during contact with metal induced by electromagnetic energy. A three-turn coil that generates electromagnetic fields at a frequency of 100 kHz was used. The temperature increases in metal plates and skin tissue during electromagnetic field exposure were calculated using a numerical simulation of Maxwell's equation and the bioheat model. The effects of plate material, plate thickness, coil distance, and exposure time on skin temperature increases were systematically investigated. Three different types of materials, namely iron, aluminum, and copper, were chosen for this study. The highest temperature increases in the skin in relation to the threshold temperature for generating skin injury were investigated.

## 2. Formulation of the Problem

A time-varying electromagnetic field is caused by alternating currents. This field induces currents in neighboring conductors. Eddy currents are the name given to induced currents. Different metals and exposure distances result in differences in the resulting electromagnetic distribution pattern and power absorption in nearby metal objects. However, the heat transfer characteristics and tissue temperature increase caused by contact with electromagnetically heated metal are not well established. A systematic study of different metals exposed that interact with body tissue is required to adequately explain the thermal effects of tissue, which are associated with the electromagnetic energy absorption of the attached metal. Figure 2 shows the skin heating caused by contact with highly conductive metallic material during exposure to near-field electromagnetic energy from electronic equipment. The tissue that was in contact with the metal plate was placed over an induction coil, which produces time-varying electromagnetic fields. They were surrounded by air, and there was an air gap between the coils and the tissue. The consequence of tissue in contact with metal, when subjected to an alternating electromagnetic field, is an increase in tissue temperature, which results from metals absorbing the energy obtained through induction. This study aimed to assess the spatial and temporal temperature increases within skin tissue due to thermal contact with highly conductive metallic materials when subjected to high-intensity electromagnetic energy exposure. Heat exchange between the human body and the surrounding thermal environment encompasses conduction, convection, radiation, and evaporation as the primary mechanisms, while contact conductance facilitates heat transfer between the metal plate and the skin surface.

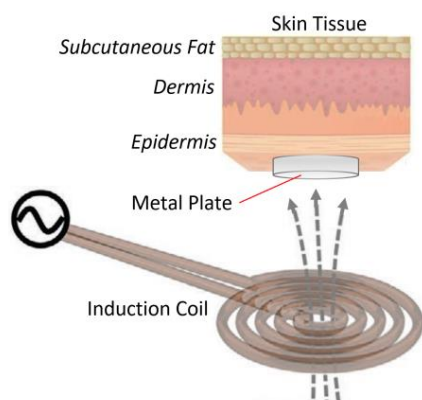


**Figure 2.** Skin heating due to contact with a highly conductive metallic material while exposed to high-intensity electromagnetic fields.

**3. Methods and Model**

Electromagnetic induction heating is comparable to the Joule heating effect, but with one significant difference: The currents that heat the material are induced through electromagnetic induction. This process is a nonlocal, or no-contact, heating process. A time-varying magnetic field is produced by delivering a high-frequency alternating current via an induction coil. The material to be heated is positioned in the magnetic field without being in contact with the coil. It is important to note that not all materials can be heated by induction; only those with high electrical conductivity can (such as copper, gold, and iron). The alternating electromagnetic field induces eddy currents in the material, resulting in resistive losses that heat it up. Electromagnetic induction heats ferrous metals more effectively than other materials. This is due to their high permeability, which increases the production of eddy currents and skin effects. Furthermore, another heating mechanism takes place. The iron crystals in the material are magnetized and demagnetized repeatedly by the alternating magnetic field. This causes the magnetic domains to flip back and forth rapidly, resulting in hysteresis losses and additional heat.

The objective of this research was to estimate the thermal response of the skin when in contact with metal under the influence of electromagnetic energy. Figure 3 shows the physical representation of this study, where interactions between the tissue model and the electromagnetic field emitted by the induction coil took place. The first step in assessing the effects of electromagnetic fields is to determine the induced and spatial distribution of the fields in the model generated by the induction coil. After that, energy absorption, which causes a temperature increase in the metal plate and tissue, as well as other interactions, could be evaluated.

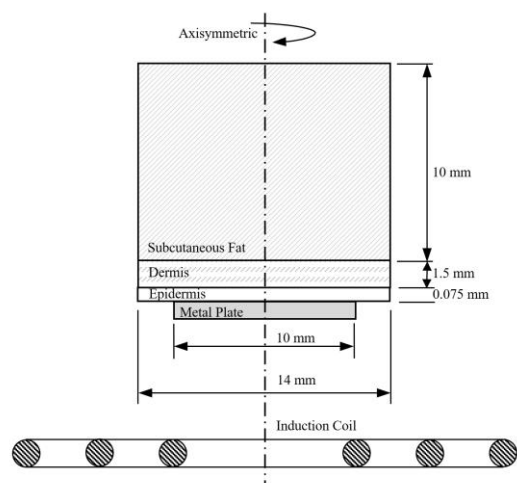


**Figure 3.** Physical model of the problem.

### 3.1. Physical Model

To investigate the thermal response of skin tissue in contact with a metal plate to electromagnetic energy and the temperature increase in tissue, a multi-layered skin model was exposed to an induction coil. To decrease processing time while maintaining resolution, a 2D axisymmetric model was employed in this work to represent a vertical cross-section of a 3D model. The multi-layered skin model had dimensions of 14 mm in width and 11.575 mm in height [11]. This model was comprised of three types of tissues: Epidermis, dermis, and subcutaneous fat. These tissues differ in their dielectric and thermal properties. Table 1 shows the dielectric and thermal properties of the tissues based on a comprehensive literature review. Each tissue was assumed to be homogeneous, as well as electrically and thermally isotropic. The chemical reaction and phase change within the tissue were unaffected. The metal plate in contact with the skin was 10 mm wide. The induction coil is in front of the skin segment at different distances. The alternating current signal excited the induction coil, resulting in Joule heating and hysteresis loss. The induction coil delivered 5 W of power at a frequency of 100 kHz. The induction coil configuration had three turns and a coil diameter of 2 mm. Copper was used for the induction coil fabrication because of its high electrical conductivity (low power losses), high thermal conductivity (easily cooled with water), and inexpensive cost. The physical model and specifications of the induction coil used in this study are depicted in Figure 3.

**Table 1.** Material properties [2,11,32].

Material	Density ( $\rho$ ) (kg/m <sup>3</sup> )	Thermal Conductivity ( $k$ ) (W/m·K)	Heat Capacity ( $C$ ) (J/kg·°C)	Blood Perfusion Rate ( $\omega_b$ ) (1/s)	Electrical Conductivity ( $\sigma$ ) (S/m)	Relative Permittivity ( $\epsilon_r$ )	Relative Permeability ( $\mu_r$ )
Epidermis	1200	0.21	3600	0.024	1.18	38.9	1
Dermis	1200	0.37	3600	0.024	1.18	38.9	1
Subcutaneous fat	900	0.16	2500	0.00058	0.19	11.0	1
Iron	7870	71.97	448	-	$1.17 \times 10^7$	1	300
Aluminum	2698	225.94	921	-	$3.5 \times 10^7$	1	1
Copper	8960	400	385	-	$5.96 \times 10^7$	1	0.999994
Air	1.29	0.025	1004	-	0	1	1

### 3.2. Equations for Electromagnetic Field Analysis

The mathematical models represent the electromagnetic field and its oscillations, as well as the physiological processes that result from interactions between the electromagnetic field and materials. The following assumptions were made to simplify the problem:

1. The electromagnetic field was modeled in a 2D axisymmetric geometry.
2. The electromagnetic field was interacting with the metal and tissue in the open space.
3. The free space was truncated by an infinite element domain.
4. The model assumes that the dielectric properties of metal and tissue are constant.

To explain the propagation of electromagnetic fields over a medium, Maxwell equations were used, which mathematically expressed the interdependence of electromagnetic phenomena. To demonstrate the electromagnetic field that penetrates the medium during induction heating, the simplified Maxwell equations [32] were adopted as follows:

$$\nabla \times \mathbf{H} = \mathbf{J} \quad (1)$$

$$\mathbf{B} = \nabla \times \mathbf{A} \quad (2)$$

$$\mathbf{E} = -j\omega\mathbf{A} \quad (3)$$

$$\mathbf{J} = \sigma\mathbf{E} + j\omega\mathbf{D} \quad (4)$$

where  $\mathbf{H}$  is the magnetic field intensity (A/m),  $\mathbf{B}$  is the magnetic flux density (T),  $\mathbf{E}$  is the electric field intensity (V/m),  $\mathbf{A}$  is the magnetic vector potential (Wb/m),  $\mathbf{D}$  is the electric displacement or electric flux density (C/m<sup>2</sup>),  $\mathbf{J}$  is the electric current density (A/m<sup>2</sup>),  $\sigma$  is the electrical conductivity of the material (S/m),  $j = \sqrt{-1}$  and  $\omega = 2\pi f$ ; is the angular frequency of the magnetic field (rad/s).

A generalized form of the constitutive relationships between electric field intensity and electric displacement can be described as:

$$\mathbf{D} = \varepsilon_0 \varepsilon_r \mathbf{E} \quad (5)$$

where  $\varepsilon_0$  is the permittivity of free space ( $8.8542 \times 10^{-12}$  F/m),  $\varepsilon_r$  is the relative permittivity (dimensionless).

Similarly, a generalized form of the constitutive relationships between magnetic field intensity and magnetic flux density can be described as:

$$\mathbf{B} = \mu_0 \mu_r \mathbf{H} \quad (6)$$

where  $\mu_0$  is the permeability of free space ( $1.257 \times 10^{-6}$  H/m), and  $\mu_r$  is the relative permeability (dimensionless).

For the inductor, the current density in the direction of the wires is defined as:

$$\mathbf{J}_e = \frac{N(V_{coil} + V_{ind})}{AR_{coil}} \mathbf{e}_{coil} \quad (7)$$

Electromagnetic phenomena are inherently scattered over an endless space. The outer layer of the calculated domain, i.e., the free space, was truncated by an infinite element. The outer boundary of the calculated domain was considered a magnetic insulation boundary condition to eliminate reflections:

$$\mathbf{n} \times \mathbf{A} = 0 \quad (8)$$

where  $\mathbf{n}$  is the normal vector.

### 3.3. Equations for Heat Transfer Analysis

The heat transfer and temperature rise of tissue in contact with metal caused by electromagnetic near-field exposures were investigated in this work. The coupled effects of an electromagnetic field and transient heat transfer were solved. The temperature increase in the tissue was caused by the absorption of electromagnetic energy by the metal. The absorbed electromagnetic energy in the metal plate was then transmitted to the skin tissue. The following assumptions were made to simplify the complexity of the problem:

1. The heat transport was represented by a 2D axisymmetric geometry.
2. The tissue and metal had constant thermal properties.
3. During the exposure, no material phases changed.
4. There was no chemical response in the tissue.
5. The tissue was homogeneous and thermally isotropic.

Heat transfer via the attached metal plate was considered heat conduction in a homogeneous medium. The transient conduction heat equation, provided by Equation (9), is employed to govern the transfer of heat in the metal plate.

$$\rho C \frac{\partial T}{\partial t} = \nabla \cdot (k \nabla T) + Q_e \quad (9)$$

The electromagnetic heat source,  $Q_e$  (W/m<sup>3</sup>), in the heat equation combines resistive and magnetic losses.

$$Q_e = Q_{rh} + Q_{ml} \quad (10)$$

where the resistive losses ( $Q_{rh}$ ) are

$$Q_{rh} = \frac{1}{2} \text{Re}(\mathbf{J} \cdot \mathbf{E}) \quad (11)$$

and the magnetic losses ( $Q_{ml}$ ) are

$$Q_{ml} = \frac{1}{2} \text{Re}(i\omega \mathbf{B} \cdot \mathbf{H}) \quad (12)$$

The skin model was considered a biomaterial with circulating blood. The temperature increase in skin tissue is determined by solving Pennes' bioheat equation [28]. The transient bioheat equation efficiently represents how thermal energy exchange occurs within tissue and can be stated as follows:

$$\rho C \frac{\partial T}{\partial t} = \nabla \cdot (k \nabla T) + \rho_b C_b \omega_b (T_b - T) + Q_{met} + Q_e \quad (13)$$

where  $\rho$  is the tissue density ( $\text{kg}/\text{m}^3$ ),  $C$  is the heat capacity of the tissue ( $\text{J}/\text{kg} \cdot \text{K}$ ),  $k$  is the thermal conductivity of the tissue ( $\text{W}/\text{m} \cdot \text{K}$ ),  $T$  is the tissue temperature ( $^{\circ}\text{C}$ ),  $T_b$  is the temperature of the blood ( $^{\circ}\text{C}$ ),  $\rho_b$  is the density of the blood ( $\text{kg}/\text{m}^3$ ),  $C_b$  is the heat capacity of the blood ( $\text{J}/\text{kg} \cdot \text{K}$ ),  $\omega_b$  is the blood perfusion rate ( $1/\text{s}$ ),  $Q_{met}$  is the metabolic heat source ( $\text{W}/\text{m}^3$ ), and  $Q_e$  is the external heat source (the electromagnetic heat source) ( $\text{W}/\text{m}^3$ ). The blood perfusion term,  $\rho_b C_b \omega_b (T_b - T)$ , approximates heat conduction between the tissue and the blood flow in this analysis.

The heat transfer analysis discarded the surrounding air and was limited to the skin and metal plate. The skin surface, as shown in Figure 3, was considered the convective boundary condition, where the convection heat transfer coefficient between the skin and the air was  $7 \text{ W}/\text{m}^2 \cdot \text{K}$ . The cooling provided by sweat evaporation from the skin surface was  $10 \text{ W}/\text{m}^2$  at an ambient temperature of  $25 \text{ }^{\circ}\text{C}$  [11]. Assuming that the heat loss due to radiation was negligible, the boundary condition here can be written as:

$$-n \cdot (-k \nabla T) = h_{am}(T - T_{am}) + E_{vap} \quad (14)$$

where  $T_{am}$  is the ambient temperature ( $^{\circ}\text{C}$ ), and  $h_{am}$  is the ambient convection coefficient ( $\text{W}/\text{m}^2 \cdot \text{K}$ ) and  $E_{vap}$  is the heat loss due to the sweat evaporation.

The heat was exchanged between the metal plate and the skin surface via contact conductance. The contact conductance between tissue and metallic surface ( $h_{contact}$ ) was set to  $9000 \text{ W}/\text{m}^2 \cdot \text{K}$  [12] for all cases in this study. This value has been proven to be sufficiently high to accurately represent the heat exchange between the tissue and metallic surfaces, and it ensures that the resulting temperatures within the epidermis are well within an acceptable range of accuracy. The boundary condition stated below is employed.

$$-n \cdot (-k \nabla T) = -h_{contact} (T_{metal} - T_{epidermis}) \quad (15)$$

where  $T_{metal}$  is the metal temperature ( $^{\circ}\text{C}$ ),  $T_{epidermis}$  is the epidermis temperature ( $^{\circ}\text{C}$ ) and  $h_{contact}$  is the contact conductance ( $\text{W}/\text{m}^2 \cdot \text{K}$ ).

It is assumed that no contact resistance exists between the internal layers of skin tissue. Therefore, the internal boundaries are assumed to be continuous:

$$n \cdot (k_u \nabla T_u - k_d \nabla T_d) = 0 \quad (16)$$

$$T_u = T_d \quad (17)$$

The boundaries on the left and right sides of the skin tissue are considered to be thermally insulated [11]:

$$-n \cdot (-k \nabla T) = 0 \quad (18)$$

In the beginning, the temperature distribution within the tissue was assumed to be uniform at the body core temperature of 37 °C. Therefore, the temperature boundary condition of 37 °C is applied to the deep tissue surface, where the skin model was truncated.

#### 3.4. Calculation Procedure

The finite element method (FEM) was utilized to numerically solve the system of governing equations and initial as well as boundary conditions. The numerical problem was solved using the adaptive mesh refinement approach. The computational problem was addressed using COMSOL™ Multiphysics (<https://cn.comsol.com/>, accessed on 24 June 2023) to investigate the processes that occurred in the skin model under exposure to an electromagnetic field. Figure 4 demonstrates the computational domain using triangular element meshes with a boundary perfectly matched layer (PML) for effective truncation and absorption of electromagnetic fields (EMF). A mesh convergence analysis was conducted to determine the optimal number of elements needed for the study. The convergence curve, depicted in Figure 5, resulted from this analysis. Based on the convergence test, a grid consisting of approximately 10,000 elements was deemed appropriate. It can be reasonably assumed that, beyond this element count, the accuracy of the simulation results remains unaffected by the number of elements. The time step was dynamically determined by the Solver using an adaptive algorithm to ensure accurate and efficient simulation results.

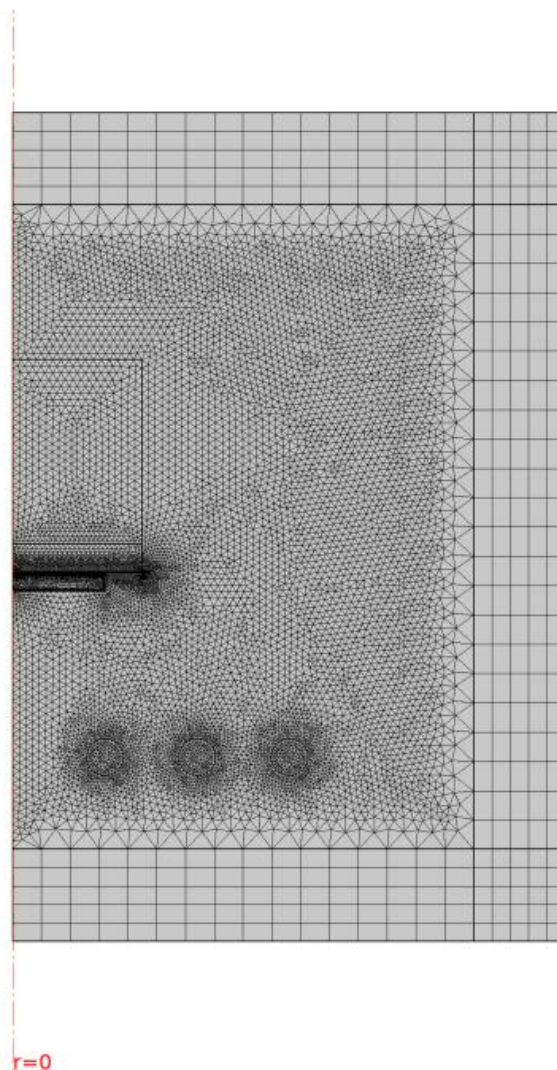


**Figure 4.** A two-dimensional axisymmetric finite element mesh of the model.

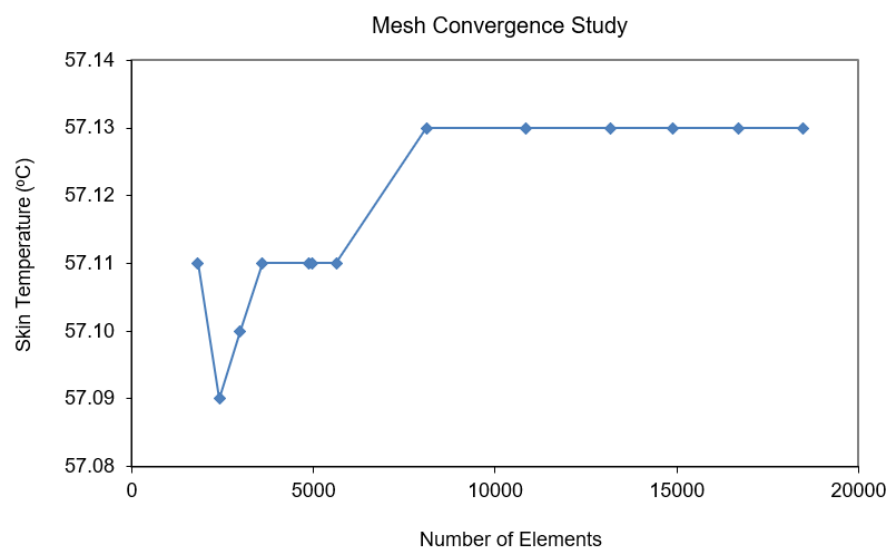


**Figure 5.** Mesh convergence study of the model.

#### 4. Results and Discussion

The induction coil (inductor) to which the alternating current was applied was utilized to generate an electromagnetic field with a specified pattern that heats an electrically conductive item such as a metal plate. All the analysis and corresponding results presented in this study were obtained using a frequency of 100 kHz. The magnetic field, electric field, and temperature distributions in the skin tissue and metal plate during exposure to electromagnetic energy were obtained by the numerical simulation of Maxwell's equation and Pennes' bioheat equation. The exposure condition considered in this study referred to the threshold temperature for producing skin damage of 43 °C [3,4]. The effects of plate material, plate thickness, coil distance, and exposure time on the temperature increase in the skin tissue were numerically investigated.

##### 4.1. Verification of the Model

To validate the model proposed here, the simple case of the simulated results was validated against the numerical results obtained by Ng et al. [11] using the same geometric model. The skin temperature was determined in a three-layered skin tissue model in contact with a heated metal plate. The temperature of the heating plate was set to 90 °C in the validation case. The validation test result is shown in Figure 6 and indicates strong agreement of the steady-state temperature with the distance between the current solution and that of Ng. The temperature was highest on the skin's surface closest to the heated metal plate (on the right side of the graph) and gradually decreased as skin layer depth increased. This favorable comparison strengthens our confidence in the accuracy of the current numerical model, particularly in faithfully representing the intricate processes that occur during the interaction between human skin and a metal plate heated through electromagnetic induction from an external source.

##### 4.2. Effect of Plate Material

The coupled effects of electromagnetic near-field distribution and unsteady bioheat transfer as well as initial and boundary conditions were investigated to analyze heat transfer in skin tissue. Due to these coupled effects, the intensity of the electric field in Figure 7a and the magnetic field in Figure 7b were converted into heat in Figure 7c by hysteresis and Joule heating from eddy currents. In the condition of skin contact with the 1 mm metal plate, 1 cm exposure distance, and 5 W of power, the high-temperature zone in Figure 7c went deep into the dermal layer but did not penetrate through the dermis to the subcutaneous fat.

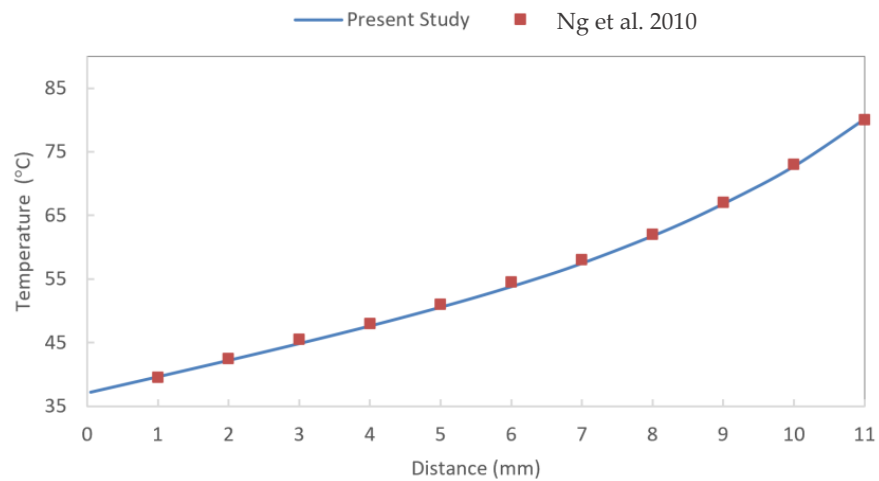


**Figure 6.** Comparison of the calculated temperature distribution to the temperature distribution obtained by Ng et al. [11].

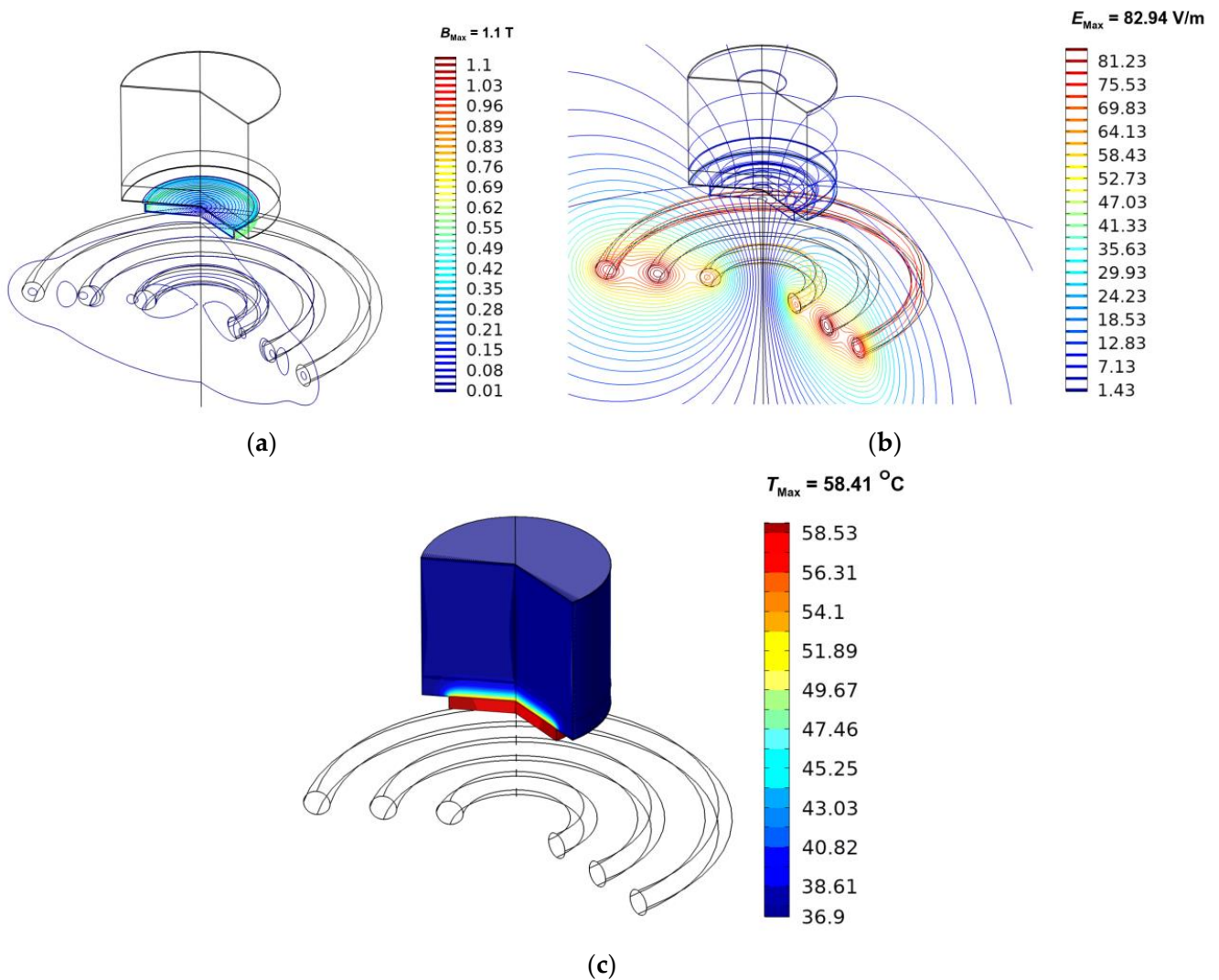


**Figure 7.** Distribution of magnetic field (a), electric field (b), and temperature (c) when skin is in contact with a 1 mm-thick iron plate for 10 s.

The effect of plate material was investigated for three different sample materials. The dielectric and thermal characteristics of the plate are crucial parameters in the increase of

skin temperature during electromagnetic field exposure. Figure 8 shows the variation of skin surface temperature with different plate thicknesses and materials. According to the graph, iron was the most sensitive material to heat via electromagnetic induction, followed by aluminum and copper. To obtain the same temperature as iron for aluminum and copper, several times as much power would be necessary. The main causes of the differences were variations in the electrical resistivity and magnetic permeability of the metals. Copper's lower resistivity (high conductivity) requires substantially more current to provide the same transmission losses or resistive losses (Joule heating) as iron. Copper has excellent electrical conductivity with low electrical resistivity. As a result, it exhibits minimal Joule heating effects since it conducts current efficiently, leading to lower electrical resistance and less heat generation. Aluminum alloys typically have a higher electrical resistivity than pure copper, but a lower one than iron. Consequently, they generate intermediate Joule heating effects. Iron has moderate electrical resistivity, which results in moderate Joule heating effects. Iron also has a higher magnetic permeability (Table 1), allowing it to be heated using hysteresis in addition to Joule heating.

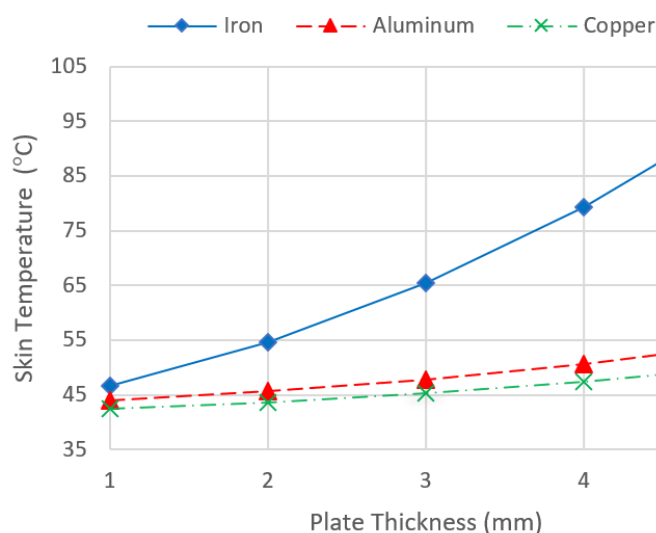


**Figure 8.** Skin surface temperature variation with different plate thicknesses and materials.

#### 4.3. Effect of Plate Thickness

The effect of plate thickness was also studied. Figure 8 shows a comparison of skin temperature with different plate thicknesses. For the iron plate, the maximum skin temperature increases are 46.7 °C, 54.6 °C, 65.4 °C, 79.4 °C, and 96.5 °C for the plate thickness of 1 mm, 2 mm, 3 mm, 4 mm, and 5 mm, respectively. It was found that the larger plate thickness corresponds to a higher temperature increase in skin tissue. This was because, during electromagnetic energy exposure, the metal plate acted as a thermal energy transmitter, transferring heat to the skin tissue. The higher metal thickness allowed a greater amount of heat generation in the metal object due to Joule and hysteresis losses. Moreover, the greater the metal thickness, the greater the amount of heat generated and transferred to the skin tissue due to Joule and hysteresis losses during electromagnetic energy exposure. In all cases, the highest skin temperature occurred near the skin surface, close to the metal plate, where heat transfer mechanisms transmitted energy from the surface into the inner layer of skin tissue, as shown in Figure 7c. It can be concluded that when skin tissue is in contact with the metal plate while exposed to an electromagnetic field, the metal plate thickness influences skin tissue temperature increases.

#### 4.4. Effect of Coil Distance

In the model, the effect of distance from the coil on skin tissue temperature increase was systematically studied. Figure 9 shows the temperature of the skin in contact with

metal during exposure to an electromagnetic field from an induction coil at various exposure distances. Near-field electromagnetic absorption is different from far-field absorption and varies with distance from the source. According to Figure 9, the exposure distance between the coil and the skin tissue had a strong influence on skin temperature. The amount of electromagnetic heat generated in a metal plate was proportional to the intensity of the electric field ( $E$ ) and magnetic field ( $H$ ), as represented by Equations (10) and (11). As a result, the temperature induced in Figure 7c was strongly influenced by the magnetic field distribution in Figure 7a and the electric field distribution in Figure 7b. The temperature increases in the skin, as shown in Figure 9, were substantially dependent on the distance from the coil to the skin for all metals. In close proximity to the coil at 1 cm, skin temperatures rose to 57.14 °C, 56.24 °C, and 48.62 °C when contacted with iron, aluminum, and copper, respectively. The temperatures obtained at 1.0 cm exposure distances were higher than the 43 °C threshold temperature of the IEC for causing skin injury [4]. The skin temperature reduced sharply as the distance from the coil increased. This was due to the strong inductive effects in the near-field region, which increased the amount of energy absorbed very quickly with distance. Furthermore, the shorter exposure distance resulted in stronger electric and magnetic fields, and the intense heat generation in the metals distributed thermal energy to the skin tissue.

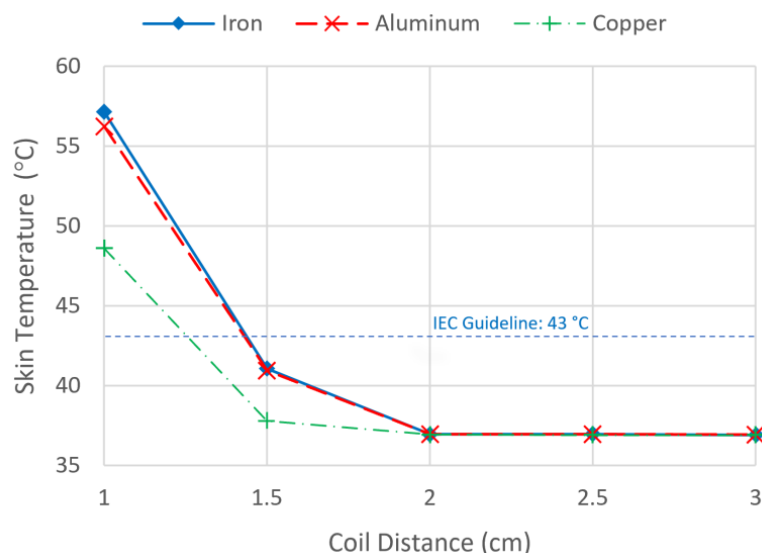


**Figure 9.** Skin surface temperature variation with different coil distances and materials.

#### 4.5. Effect of Exposure Time

To investigate the effect of exposure time, the skin was exposed to an electromagnetic field for 20 min, the metal plate with a thickness of 1 mm was attached to the skin, and the coil was fixed at 2 cm. Figure 10 shows the comparison of skin temperature increases caused by contact with three different plate materials during exposure to electromagnetic fields at various exposure times. In all cases, it took approximately 5 min to achieve a steady-state temperature. The skin temperature in contact with the iron plate was continuously the highest, followed by the aluminum plate, and the copper plate was the lowest. In this situation, the heat of iron and aluminum caused the skin temperature to exceed the IEC guideline of 43 °C [4] after more than 2 min, whereas copper caused the skin temperature to always remain below the acceptable values. The temperature increases were as expected and correspond with the results in Figures 8 and 9. According to the results, exposure time has a substantial influence on the temperature increase in the skin. The longer the exposure time, the more heat accumulates inside the skin, raising its temperature.

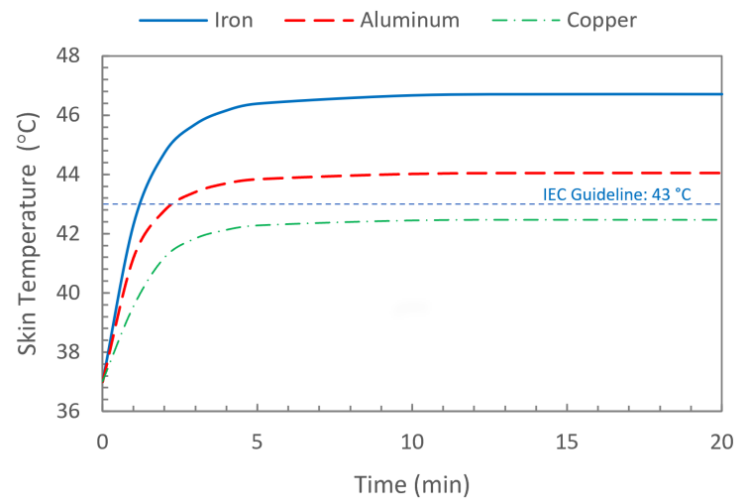


**Figure 10.** Variation in skin surface temperature with exposure time and materials.

Figure 11 depicts the distribution of skin tissue temperature following a 20 min exposure to electromagnetic energy while in contact with different metal plates: (a) Copper plate, (b) aluminum plate, and (c) iron plate. In all scenarios, the epidermis and dermis layers experienced the most significant temperature increase due to direct contact with the metal plates and the resulting heat conduction. Notably, only a small fraction of the temperature rise extended into the subcutaneous fat layer, indicating that the majority of the temperature elevation resulting from the interaction between electromagnetic energy and the metal plates was confined to the superficial layers of the skin. However, it is important to mention that the iron plate exhibited a higher capacity for heat generation compared to the other two metals, allowing a larger proportion of the heat to penetrate into the subcutaneous fat layer, thereby resulting in a deeper impact on temperature.

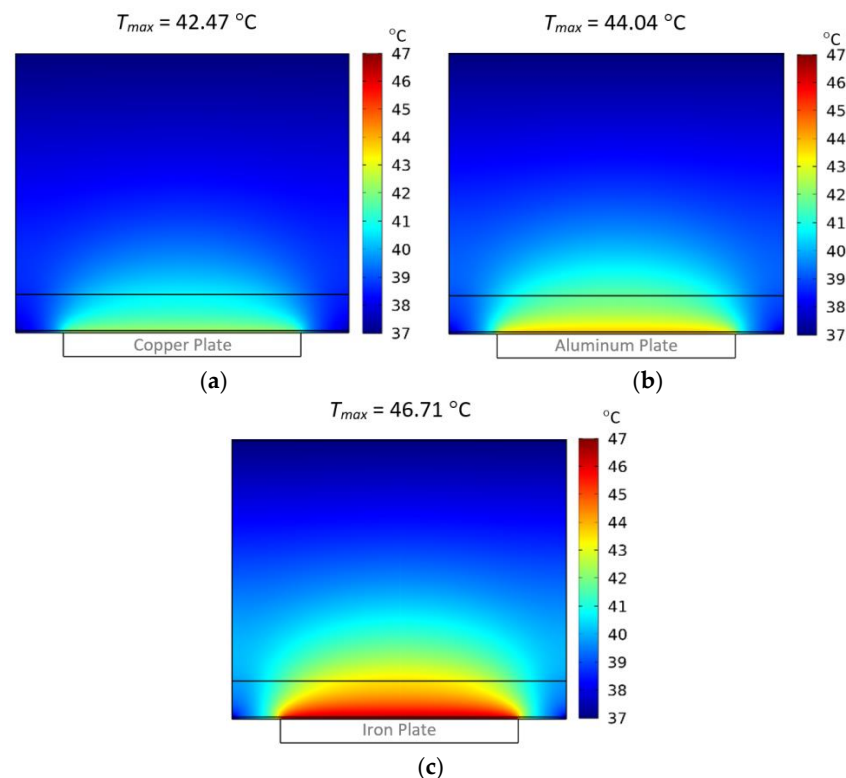


**Figure 11.** Skin tissue temperature distribution after 20 min of exposure to electromagnetic energy in contact with different metal plates: (a) copper plate, (b) aluminum plate, and (c) iron plate.

## 5. Conclusions

In this work, numerical simulations of the electric field, magnetic field, and temperature distributions in the skin in contact with metal during electromagnetic field exposure were performed. Due to the coupled effects of electromagnetic near-field distribution and unsteady bioheat transfer as well as initial and boundary conditions, the intensity of the electric field and magnetic field were converted into heat by hysteresis and Joule heating from eddy currents. The high-temperature zone reached far into the dermal layer but did not penetrate through the dermis to the subcutaneous fat in the cases examined here. At very high frequencies, such as those considered in reference [19], the electromagnetic field (EMF) would indeed primarily heat human tissues. In this frequency range, the coupling between the electromagnetic heating (dielectric heating) and the bio-heat transfer becomes significant, as the EMF directly affects the temperature distribution within the human skin. However, at low frequencies in this study, the coupling primarily concerns the metallic plate itself. Electromagnetic induction heating primarily affects the temperature distribution and heat transfer within the metallic plate and surrounding tissue, while the dielectric heating of human skin becomes less significant.

The results demonstrated various essential facts relating to energy absorption and temperature increase in the multi-layered human skin in contact with different metals during electromagnetic field exposure. The energy absorbed and skin temperature increase were strongly influenced by plate material, plate thickness, coil exposure distance, and exposure time. The most important parameter was found to be the metal type. Iron had the greatest effect on skin temperature when subjected to external electromagnetic induction. The higher metal thickness allowed for a greater amount of heat generation in the metal plate. Moreover, the greater the metal thickness, the greater the amount of heat generated and transferred to the skin tissue due to Joule and hysteresis losses during electromagnetic energy exposure. The skin temperature reduced sharply as the distance from the coil increased. In all cases, the skin temperature in contact with the metals took approximately 5 min to reach a steady-state temperature. Skin temperatures at 1.0 cm exposure distances or closer are higher than the threshold temperature for inducing skin injury for all metals when 5 W of power is applied at a frequency of 100 kHz. These results allow the researchers to estimate the exposure limits more precisely for induction coils. The findings of this study may be useful for estimating exposure limits for the power output of electromagnetic devices and their interactions with humans.

**Author Contributions:** Conceptualization, T.W.; investigation, T.W.; software, P.M. and P.R.; writing—original draft preparation, T.W.; project administration, T.W. and P.R.; funding acquisition, T.W. and P.R.; supervision, N.S.; resources, M.Y. and M.G. All authors have read and agreed to the published version of the manuscript.

**Funding:** This research was supported by The Science, Research and Innovation Promotion Funding (TSRI) (Grant no. FRB660012/0168). This research block grant was managed under the Rajamangala University of Technology Thanyaburi (FRB66E0703B.1), National Research Council of Thailand (Grant Number N42A650197), Thailand Science Research and Innovation Fundamental Fund (TUFF41/2566), Thammasat University Research Fund Contract No. TUFT 26/2565.

**Data Availability Statement:** Not applicable.

**Acknowledgments:** The authors would like to express their appreciation to the anonymous reviewers for providing helpful comments and work to enhance our manuscript.

**Conflicts of Interest:** The authors declare no conflict of interest.

## References

1. Guido, K.; Kiourti, A. Wireless wearables and implants: A dosimetry review. *Bioelectromagnetics* **2020**, *41*, 3–20. [[CrossRef](#)]
2. Ju, Y.S. Thermal management and control of wearable devices. *iScience* **2022**, *25*, 104587. [[CrossRef](#)] [[PubMed](#)]

3. Johnson, N.N.; Abraham, J.P.; Helgeson, Z.I.; Minkowycz, W.J.; Sparrow, E. An archive of skin-layer thicknesses and properties and calculations of scald burns with comparisons to experimental observations. *J. Therm. Sci. Eng. Appl.* **2011**, *3*, 011003. [[CrossRef](#)]
4. IEC 60601-2-33; Particular Requirements for the Safety of Magnetic Resonance Equipment. IEC: Geneva, Switzerland, 2010.
5. Fu, M.; Weng, W.G.; Yuan, H.Y. Numerical simulation of the effects of blood perfusion, water diffusion, and vaporization on the skin temperature and burn injuries. *Numer. Heat Transf. Part A Appl.* **2014**, *65*, 1187–1203. [[CrossRef](#)]
6. Monds, J.R.; McDonald, A.G. Determination of skin temperature distribution and heat flux during simulated fires using Green's functions over finite-length scales. *Appl. Therm. Eng.* **2013**, *50*, 593–603. [[CrossRef](#)]
7. Yang, J.; Su, Y.; Song, G.; Li, R.; Xiang, C. A new approach to predict heat stress and skin burn of firefighter under low-level thermal radiation. *Int. J. Therm. Sci.* **2019**, *145*, 106021. [[CrossRef](#)]
8. Abraham, J.P.; Hennessey, M.P.; Minkowycz, W.J. A simple algebraic model to predict burn depth and injury. *Int. Commun. Heat Mass Transf.* **2011**, *38*, 1169–1171. [[CrossRef](#)]
9. Log, T. Analysis of Expected Skin Burns from Accepted Process Flare Heat Radiation Levels to Public Passersby. *Energies* **2021**, *14*, 5474. [[CrossRef](#)]
10. Subramanian, B.; Chato, J.C. Safe touch temperatures for hot plates. *J. Biomech. Eng.* **1998**, *120*, 727–736. [[CrossRef](#)]
11. Ng, E.Y.K.; Tan, H.M.; Ooi, E.H. Prediction and parametric analysis of thermal profiles within heated human skin using the boundary element method. *Philos. Transact. A Math. Phys. Eng. Sci.* **2010**, *368*, 655–678. [[CrossRef](#)]
12. Abraham, J.P.; Stark, J.; Gorman, J.; Sparrow, E.; Minkowycz, W.J. Tissue burns due to contact between a skin surface and highly conducting metallic media in the presence of inter-tissue boiling. *Burns* **2019**, *45*, 369–378. [[CrossRef](#)]
13. Virtanen, H.; Huttunen, J.; Toropainen, A.; Lappalainen, R. Interaction of mobile phones with superficial passive metallic implants. *Phys. Med. Biol.* **2005**, *50*, 2689–2700. [[CrossRef](#)] [[PubMed](#)]
14. Virtanen, H.; Keshvari, J.; Lappalainen, R. The effect of authentic metallic implants on the SAR distribution of the head exposed to 900, 1800 and 2450 MHz dipole near field. *Phys. Med. Biol.* **2007**, *52*, 1221–1236. [[CrossRef](#)]
15. Whittow, W.G.; Edwards, R.M. A study of changes to specific absorption rates in the human eye close to perfectly conducting spectacles within the radio frequency range 1.5 to 3.0 GHz. *IEEE Trans. Antenn. Propag.* **2004**, *52*, 3207–3212. [[CrossRef](#)]
16. Whittow, W.G.; Panagamuwa, C.J.; Edwards, R.M. The energy absorbed in the human head due to ring-type jewelry and face-illuminating mobile phones using a dipole and a realistic source. *IEEE Trans. Antenn. Propag.* **2008**, *56*, 3812–3817. [[CrossRef](#)]
17. Whittow, W.G.; Panagamuwa, C.J.; Edwards, R.M.; Vardaxoglou, J.C. On the effects of straight metallic jewellery on the specific absorption rates resulting from face-illuminating radio communication devices at popular cellular frequencies. *Phys. Med. Biol.* **2008**, *53*, 1167–1182. [[CrossRef](#)] [[PubMed](#)]
18. Mat, M.H.; Malek, M.F.A.; Whittow, W.G.; Bibb, R. Ear prosthesis evaluation: Specific absorption rate levels in the head due to different angles and frequencies of electromagnetic exposure. *J. Electromagn. Waves Appl.* **2015**, *29*, 514–524.
19. Wessapan, T.; Rattanadecho, R. Temperature induced in human organs due to near-field and far-field electromagnetic exposure effects. *Int. J. Heat Mass Transf.* **2018**, *119*, 65–76. [[CrossRef](#)]
20. Wessapan, T.; Rattanadecho, R. Temperature induced in the testicular and related tissues due to electromagnetic fields exposure at 900 MHz and 1800 MHz. *Int. J. Heat Mass Transf.* **2016**, *102*, 1130–1140. [[CrossRef](#)]
21. Bhargava, D.; Leeprechanon, N.; Rattanadecho, R.; Wessapan, T. Specific absorption rate and temperature elevation in the human head due to overexposure to mobile phone radiation with different usage patterns. *Int. J. Heat Mass Transf.* **2019**, *130*, 1178–1188. [[CrossRef](#)]
22. Bhargava, D.; Rattanadecho, R.; Wessapan, T. The effect of metal objects on the SAR and temperature increase in the human head exposed to dipole antenna (numerical analysis). *Case Stud. Therm. Eng.* **2020**, *22*, 100789. [[CrossRef](#)]
23. Wessapan, T.; Rattanadecho, R. Effect of the body position on natural convection within the anterior chamber of the human eye during exposure to electromagnetic fields. *Numer. Heat Transf. Part A Appl.* **2016**, *69*, 1014–1028. [[CrossRef](#)]
24. Wessapan, T.; Rattanadecho, R. Heat transfer analysis of the human eye during exposure to sauna therapy. *Numer. Heat Transf. Part A Appl.* **2015**, *68*, 566–582. [[CrossRef](#)]
25. Wessapan, T.; Rattanadecho, R. Flow and heat transfer in biological tissue due to electromagnetic near-field exposure effects. *Int. J. Heat Mass Transf.* **2016**, *97*, 174–184. [[CrossRef](#)]
26. Wongchadukul, P.; Rattanadecho, R.; Wessapan, T. Implementation of a thermomechanical model to simulate laser heating in shrinkage tissue (effects of wavelength, laser irradiation intensity, and irradiation beam area). *Int. J. Therm. Sci.* **2018**, *134*, 321–336. [[CrossRef](#)]
27. Wessapan, T.; Rattanadecho, R. Acoustic streaming effect on flow and heat transfer in porous tissue during exposure to focused ultrasound. *Case Stud. Therm. Eng.* **2020**, *21*, 100670. [[CrossRef](#)]
28. Pennes, H.H. Analysis of tissue and arterial blood temperatures in the resting human forearm. *J. Appl. Physiol.* **1948**, *1*, 93–122, Erratum in *J. Appl. Physiol.* **1998**, *85*, 5–34. [[CrossRef](#)]
29. Tucci, C.; Trujillo, M.; Berjano, E.; Iasiello, M.; Andreozzi, A.; Vanoli, G.P. Mathematical modeling of microwave liver ablation with a variable-porosity medium approach. *Comput. Methods Programs Biomed.* **2022**, *214*, 106569. [[CrossRef](#)]
30. Adabbo, G.; Andreozzi, A.; Iasiello, M.; Netti, P.A.; Vanoli, G.P. A 3D numerical model of controlled drug delivery to solid tumor by means of mild microwave hyperthermia-activated thermo-sensitive liposomes. *Int. J. Therm. Sci.* **2023**, *193*, 108528. [[CrossRef](#)]

31. Singh, S.; Melnik, R. Domain heterogeneity in radiofrequency therapies for pain relief: A computational study with coupled models. *Bioengineering* **2020**, *7*, 35. [[CrossRef](#)]
32. Cano-Pleite, E.; Fernández-Torrijos, M.; Santana, D.; Acosta-Iborra, A. Heat generation depth and temperature distribution in solar receiver tubes subjected to induction. *Appl. Therm. Eng.* **2022**, *204*, 117902. [[CrossRef](#)]

**Disclaimer/Publisher's Note:** The statements, opinions and data contained in all publications are solely those of the individual author(s) and contributor(s) and not of MDPI and/or the editor(s). MDPI and/or the editor(s) disclaim responsibility for any injury to people or property resulting from any ideas, methods, instructions or products referred to in the content.